Plasma Sources Science and Technology

PAPER

Metal ion thruster using magnetron electron-beam bombardment (MIT-MEB)

To cite this article: Kuo-Yi Chen *et al* 2020 *Plasma Sources Sci. Technol.* **29** 065021

Plasma Sources Sci. Technol. 29 (2020) 065021 (9pp) https://doi.org/10.1088/1361-6595/ab6361

Metal ion thruster using magnetron electron-beam bombardment (MIT-MEB)

Kuo-Yi Chen[1,2], **Po-Yu Chang**[1] and **Wan-Yi Lin**[1]

[1] Institute of Space and Plasma Sciences, National Cheng Kung University, Taiwan
[2] Institute of Propulsion and Power Technology, Tsinghua University, People's Republic of China

E-mail: pchang@mail.ncku.edu.tw

Received 8 August 2019, revised 7 December 2019
Accepted for publication 18 December 2019
Published 13 July 2020

Abstract

A new concept of ion thrusters, metal ion thrusters using magnetron electron-beam bombardment (MIT-MEB) is demonstrated. Ion thrusters provide thrusts via electrostatic fields to accelerate ions. They are widely used in spacecrafts due to the high exhaust speed. Although the thrust is very little, the final velocity of the spacecraft is much higher than using traditional rockets. For propellant, inert gases are used in conventional ion thrusters. Contrarily, a metal propellant is used in MIT-MEB. The metal propellant is solid-state, high density, easy to store, and cheap. The size of the ion thrusters can be reduced dramatically. Therefore, they can be used in a small spacecraft for both attitude and orbit control, deep space exploration, and low earth orbit. The concept of electron-beam physical vapor deposition (EB-PVD) is used to generate metal ions. A metal target is bombarded and thus heated and evaporated. An electric potential accelerates thermal-emitted electrons, which ionize the metal vapor via electron-impacting ionization. The magnetic field of a permanent magnet is used to guide the accelerated electrons towards the center of the target. This increases the efficiency of the process. Particularly but not necessarily, zinc is used for propellant due to its higher vapor pressure compared with other metals at the same temperature. This means that a lower temperature is required for zinc to be vaporized. To demonstrate our concept, an ion thruster of $10.3 \pm 0.7\ \mu N$ with a power of 26.2 ± 0.7 W was constructed as a prototype. Its mass is less than 500 g, and its diameter is $\sim$50 mm. The accelerating electric potential is 1 kV. Although an optimized design was not developed yet, we demonstrated the feasibility of building metal ion thrusters for the first time. It is a new design space and unexplored method of using a metal propellant.

Keywords: ion thruster, electric propulsion, electron-beam physical vapor deposition, metal ion source

1. Introduction

Electric propulsions provide thrusts via using electromagnetic fields to accelerate ions. The main categories of electric propulsion are [1]: (1) electrothermal where the propellants are heated resistively; (2) electrostatic where propellants are ionized and accelerated by electric fields; and (3) electromagnetic where plasma is first generated then accelerated by electromagnetic forces ($\vec{j} \times \vec{B}$ forces). Examples of (1) include resistojets and arcjets. Examples of (2) include ion thrusters and Hall thrusters, which provide very high exhaust speeds. Their efficiency is the highest among the three. Examples of (3) include pulsed-plasma thrusters and magnetoplasmadynamic thrusters. We focus on ion thrusters in this paper.

In a conventional ion thruster, a heavy inert gas atom, such as xenon, is used as the propellant. It is first ionized by discharge, then accelerated by an electrostatic field. Xenon is generally used due to the following reasons: (1) it is easily ionized; (2) it has reasonably high atomic mass; (3) it is an inert gas allowing low electrode erosion. However, xenon is very expensive due to its global shortage. In addition, a high-pressure gas cylinder is needed to store xenon gas. Having a gas cylinder makes the system more dangerous, complicated, heavy, and thereby unsuitable for a small spacecraft such as CubeSats. Our alternative idea is using a solid propellant due to its high density, i.e. relatively small volume. It also eliminates high-pressure components from the system. The missing part is an efficient way to generate ions from a solid-state material. Our method is to first produce vapor from a solid, then ionize the gas via electron impact ionization.

In the semiconductor industry, there are several mature techniques for physical vapor deposition (PVD) which generates vapor from a solid. The generated vapor eventually deposits onto the substrate surface. Common PVD methods include sputtering, pulsed-laser, thermal evaporation, and electron-beam evaporation [2]. During sputter deposition, a vacuum chamber is filled with low-pressure gas, e.g., inert gas. Plasma is then generated using either DC discharges (e.g. magnetron discharges) or AC discharge (e.g. capacitively-coupled radio frequency discharge). At the same time, a negative DC bias is applied to the target so that ions are accelerated towards the target by the electric force. Particle vaporization is achieved during physical sputtering by bombarding the target surface with energetic ions. This transfers momentum to the surface atoms of the target. We do not want to apply a background gas, which requires a high-pressure gas cylinder, to the system for generating plasma. Therefore, sputtering deposition is not suitable for our design. During pulsed-laser deposition, a high-power pulsed-laser illuminates the target surface. The target surface is vaporized by absorbing the laser energy. The vapor cloud can be ionized too by absorbing laser energy. However, it requires a high-power laser, which is not compatible with a small spacecraft. During thermal evaporation, a solid target is heated until it vaporizes. A metal target can be joule heated by a transit current directly. Otherwise, the target can be placed in a tungsten boat, which is joule heated by a transit current. An additional process is still needed to ionize the vapor. Thus, such a process is not suitable for our design, either. Finally, during electron-beam evaporation, thermal-emitted electrons are generated from a heated filament. They are accelerated by an electric field. A target can be heated when these energetic electrons bombard it, by which the kinetic energy of electrons is converted to the thermal energy of the target surface. After the temperature of the target is high enough, vaporization sets off. Electrons from the same filament can be used to ionize the vapor. Therefore, an ion source from a solid target can be implemented.

According to the concept of electron-beam physical vapor deposition (EB-PVD), a metal can be bombarded and heated by accelerated thermal-emitted electrons from a heated filament. Particularly but not exclusively, zinc is used in this context. Zinc has higher vapor pressure than other metals at the same temperature [3]. In other words, a lower temperature is sufficient for zinc to be vaporized. The metal vapor can be ionized by electron impact from the same electron source. Secondary electrons and backscattered electrons produced by the bombardment of the metal target also ionize the vapor [4–7]. To increase the efficiency of vaporization and ionization, magnets are placed underneath the metal target to guide the electrons to the center of the metal surface. Therefore, a metal ion thruster using magnetron electron-beam bombardment (MIT-MEB), a new type of ion thrusters that uses high-density solid propellants and is easier to be carried on a spacecraft, is developed.

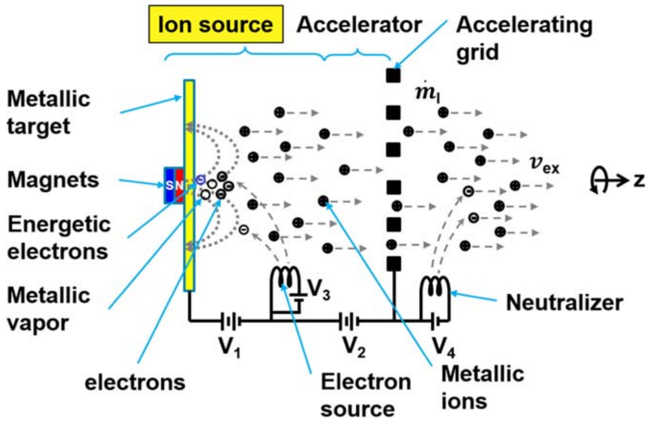

Figure 1. Scheme of MIT-MEB. The metal target is the propellant. V_3 and V_4 drive currents for heating filaments. The electrons are thermally emitted. V_1 accelerates thermal-emitted electrons from the filament in the ion source region. V_2 accelerates ions for providing thrusts in the accelerator region.

2. Concepts of the metal ion thrusters

The MIT-MEB consists of three elements typical to any ion thrusters as shown in figure 1: (i) an ion source using magnetron electron-beam bombardment, (ii) an accelerator, and (iii) a neutralizer.

(i) **The ion source:** the metal ion source using magnetron electron-beam bombardment is our main innovation in this paper, see section 2.1 for details. Ions are not only generated but also pre-accelerated by the potential V_1, which is used to accelerate electrons from the electron source for bombarding the metal target, see figure 1.

(ii) **The accelerator:** the accelerator is located downstream of the ion source. We use an electrostatic grid with negative potential away from the ion source section to accelerate ions.

(iii) **The neutralizer:** the neutralizer located downstream of the accelerator emits electrons to neutralize accelerated ions. If ions were not neutralized before leaving the thruster, the thruster would become negatively charged. In this case, the thruster not only collects ions originally in space but also attracts the accelerated ions back to the thruster cancelling the thrust. The neutralizer is made of filaments similar to the one emitting electrons in the ion source section. Thermal-emitted electrons are attracted and moved by accelerated ions. Ions are neutralized via collisions with electrons.

In this paper, the ion source is combined with the accelerator by setting V_2 in figure 1 equals zero for simple demonstrations.

2.1. The ion source section

The ion source section consists of four elements: (i) a hot tungsten filament; (ii) a metal target; (iii) an electric potential between the hot filament and the metal target; (iv) a magnetic field.

(i) **The hot tungsten filament:** it is the electron source for thermal emission. When a metal is heated, electrons escape from its surface. The current density of the thermionic current from a hot filament can be estimated by Sir Owen Willans Richardson [2, 8–10]:

$$j = \lambda_R A_0 T^2 e^{-\frac{w}{k_B T}} \tag{1}$$

where $A_0 = 4\pi m k_B^2 e/h^3 = 1.2 \times 10^6\ \mathrm{A\ m^{-2}K^{-2}}$ is a universal constant, λ_R is a factor characteristic to materials (in the order of 0.5), T is the temperature of the filament in kelvin, w is the work function of the material, and k_B is the Boltzmann constant. Notice that the current is very sensitive to the filament temperature. In other words, a roughly steady filament temperature can yield a wide range of currents. We used a tungsten filament heated by DC current due to its high melting point.

(ii) **The metal target:** a thin plate of thickness 0.5 mm made of zinc was used as a propellant. Its vapor pressure is higher than that of other metals at the same temperature [3]. Therefore, a lower temperature is required for zinc to be vaporized. It was heated, vaporized, and ionized by electron bombardment.

(iii) **The electric potential:** it is used to accelerate electrons. The metal target has a higher electric potential than the heated filament, i.e. $V_1 > 0$ in figure 1. As a result, the thermal-emitted electrons from the hot filament are accelerated towards the target. Electrons convert their kinetic energy to the target's thermal energy while bombarding the metal target. On the other hand, ions can also be pre-accelerated before entering the accelerator region.

(iv) **The magnetic field:** it is used to guide thermal-emitted electrons towards the center of the target. The magnetic field is provided by a permanent magnet underneath the target. It needs to be strong enough to magnetize the accelerated thermal-emitted electrons so that they follow the field lines and arrive at the center of the target. In contrast, ions should not be magnetized so that they are pre-accelerated and leave the ion source freely.

Electrons play a double role since they heat the target and ionize the metal vapor. When energetic electrons collide with the zinc target, there should be about 35% of them colliding with the solid target elastically and backscattered with an energy of $E_{BSE} \approx 0.51E_0 = 2.55$ keV [5–7] for $V_1 = 5$ kV used as the first condition in our experiments. For $V_1 = 1$ kV, which is the second condition used in our experiments, $E_{BSE} \approx 0.51$ keV. The rest of the electrons collide with the target inelastically and create true secondary electrons, those originally in the solid and are ejected by energies delivered by incoming-energetic electrons, with energies typically less than 15 eV [11, 12]. The true secondary electron yield is defined as the ratio between the secondary and the incoming electron counts. For incoming electrons with energy in the order of 1 keV or below, the true secondary electron yield exceeds 1 for most materials. When the energy of incoming electrons is in the order of 5 keV or above, the yield goes down to ~0.1 [11, 13]. In any case, secondary electrons, including backscattered and true secondary electrons, are confined by the electric potential and the magnetic field to a small region on top of the target surface forming an electron cloud. Their energy in the cloud is more than sufficient to ionize zinc atoms since the first ionization energy of zinc atoms is 9.4 eV [14].

2.2. Design of the metal ion thrusters

Figure 2 shows the CAD drawing, the photo of MIT-MEB, the simulated electric and magnetic field lines, the calculated gyroradius, and a photo of a target after experiments. The dimensions of MIT-MEB are $56 \times 46 \times 74\ \mathrm{mm}^3$. The mass is less than 500 g. The body of the thruster is made of ceramic due to its high melting point (over 2000 °C) and low thermal conductivity (12.6 W m^{-1} K^{-1} at 426.7 °C and it is lower when the temperature is higher [15]). The magnets are placed in the ceramic cup, while the metal target is on top of the cup, which has a thickness of 1 mm. The diameter of the magnet is 20 mm. The inner diameter of the ceramic cup and the diameter of the metal target are both 30 mm. Three identical magnets are used on top of each other. The bottom two magnets are used as space holders. The whole system will shrink without the bottom two magnets in the future. The top surface of the magnet is 1 mm below the inner surface of the top of the cup. The distance between the target surface and the magnet surface is 2.5 mm. The 1-mm gap between the magnets and the ceramic cup provides extra thermal insulation between the heated target and the magnets. This way, the temperature of the magnets is kept under the Curie temperature of ~300 °C for neodymium magnets. In addition, low heat conductivity prevents heat loss, so that the metal target can be heated and evaporated efficiently. One 10-mm long tungsten filament is placed parallel to and located at 3 mm above the target surface. It is heated to more than 1300 °C by a ~2-V DC power supply with a current of ~2 A. The target was connected to a high voltage DC power supply with $V_1 = 5$ kV or 1 kV, see figure 1. The magnetic field, shown in figure 3(a), is 0.15–0.25 T between the target (2.5 mm above the top surface of the magnet) and the filament (5.5 mm above the top surface of the magnet). We obtained the figure using a field measurement system consisting of a 3-axis manual-linear stage with a precision of 10 μm in each direction and a gaussmeter (WT10A, Weitecidian) with a precision of ±2% for magnetic fieldd below 1 T. The probe of the gaussmeter was put on a fixed stand. The magnet, on the other hand, was glued to the top surface of the stage. It was the magnet being moved by the linear stage for scanning the magnetic field at different locations, see figure 3(b). We first fixed the height of the probe. Then we moved around the magnet until we found the location with the highest magnetic field. That point was designated as the center of the magnet. We then moved the magnet sideways with a step size of 0.5 mm and measured the magnetic field at each step.

Figure 2(c) shows the simulated magnetic field lines (white), electric field lines (black), and calculated gyroradiuses

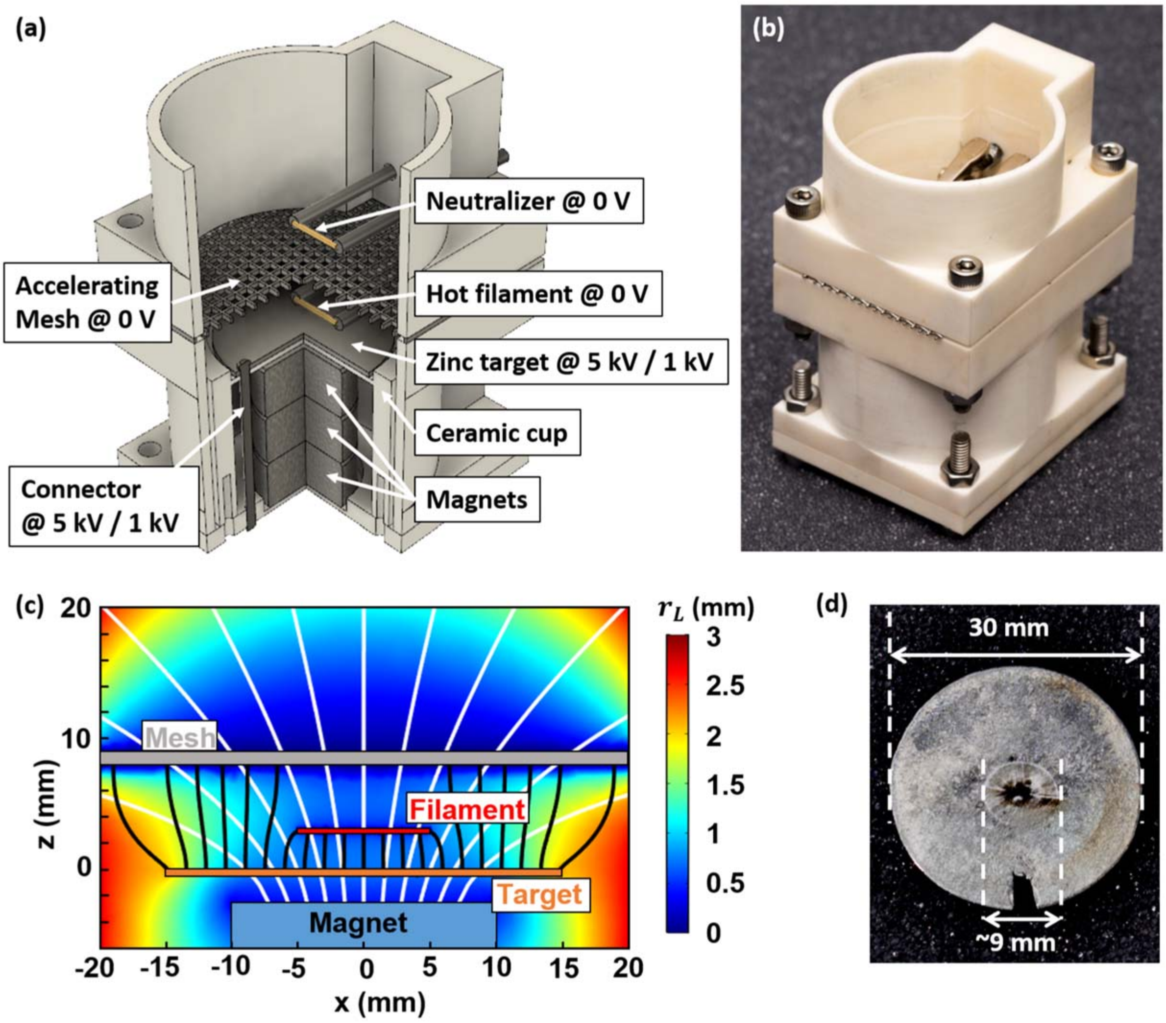

Figure 2. (a) The CAD drawing and (b) a photo for the MIT-MEB. (c) Simulated magnetic field lines (white), electric field lines (black) and the calculated gyroradiuses (color contours) for thermal-emitted from the filament. Both the filament (red) and the mesh (gray) are at ground level, while the target (orange) is at a high positive voltage (5 kV in this simulation). (d) A target after being used. The center region was bombarded by electrons, and it evaporated fully. The target melted in a circular region with a diameter of $\sim$9 mm during the experiments.

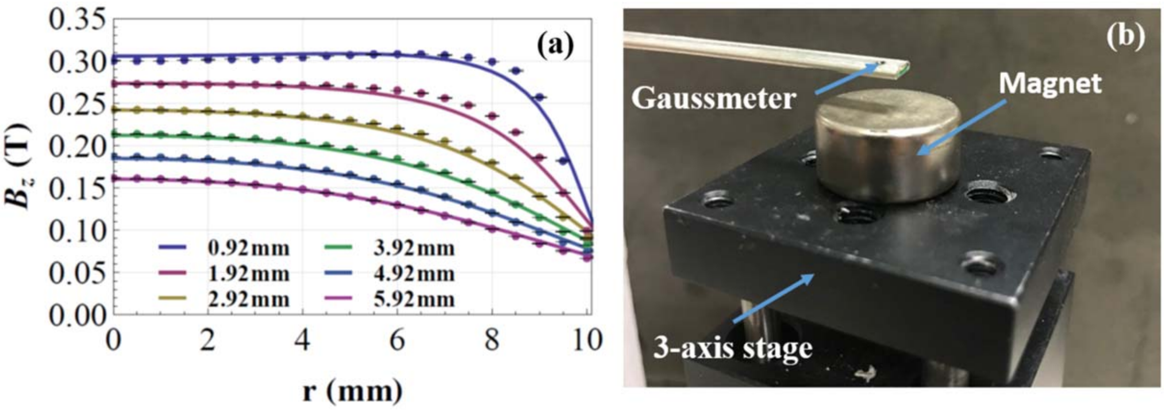

Figure 3. (a) The measured $\hat{z}$ component of the magnetic field. Points represent measurements, solid lines represent simulation. Different colors represent magnetic fields at different heights. Height is measured relative to the top surface of the magnet. The simulated magnetic field from a magnet with the same dimensions as the actual one and with a magnetization of 750 kA/m matches the measured field. (b) The field measurement system consisting of a 3-axis manual-linear stage and the gaussmeter.

of thermal-emitted electrons (color contours). We varied the magnetization of the magnet while keeping the same dimensions as the actual one until the simulated field matched the measurement. Finally, the magnetization of 750 kA/m provided the best fit to the measured fields. The simulated magnetic fields are also plotted in figure 3(a) for comparing to the measured ones, see figure 2(c). Note that the simulated fields only deviate from the measured ones at the edge of the magnet. Those points are not relevant since the hot filament for emitting electrons was only 10 mm long, i.e. within $r = 5$ mm. On the other hand, the electric fields were calculated from the electric potential obtained by solving Poisson's equation with setting the electric potential of the target to 5 kV. Since the electric potential of the hot filament is at ground level, the energy of electrons emitted from the filament can be obtained from the electric potential at their locations. With given magnetic field and electron energy at all locations, the gyroradiuses are calculated as

$$r_{\mathrm{L}} = \left| \frac{m_{\mathrm{e}} v_{\perp}}{eB} \right| \leqslant \left| \frac{m_{\mathrm{e}} v}{eB} \right| = \frac{1}{B} \sqrt{\frac{2Vm_{\mathrm{e}}}{|e|}} \qquad (2)$$

where v is the electron velocity, $v_{\perp}$ is the component of the electron velocity perpendicular to the magnetic field line, V is the simulated electric potential, m_{e} and e denote the mass and the charge of an electron, respectively, and B denotes the simulated magnetic field. As shown in figure 2(c), the gyroradiuses between the filament and the target are much smaller than the target size. This indicates that electrons are magnetized and follow the magnetic field lines towards the center of the target. When the electric potential of the target is only 1 kV, the electrons are less energetic than that in the case where 5 kV is used. The electron gyroradiuses shrink meaning that electrons are also magnetized when 1 kV is used. Therefore, they follow the same magnetic field lines. In both cases, the electrons are accelerated by the electric field on the way to the target.

Shown in figure 2(d) is a target bombarded by an electron current of ~3 mA with 5-kV accelerating voltage for 5 mins. The dark color at the center of the target represents the area heated by electron bombardment. Around the dark area, there is a round area of diameter of ~9 mm. This area was not bombarded, but it was heated via conduction. The temperature within that range was greater than the melting temperature of zinc, i.e. 419.5 °C [16]. The experiments described in section 3 showed that the zinc target mass decreased by 70 ± 10 mg after 5 mins of operation with a power of 19.0 ± 0.8 W including the power consumption for heating filaments and accelerating electrons. The evaporation rate was $\dot{m}_{\mathrm{v}} = (2.2 \pm 0.4) \times 10^{-4}$ g/s.

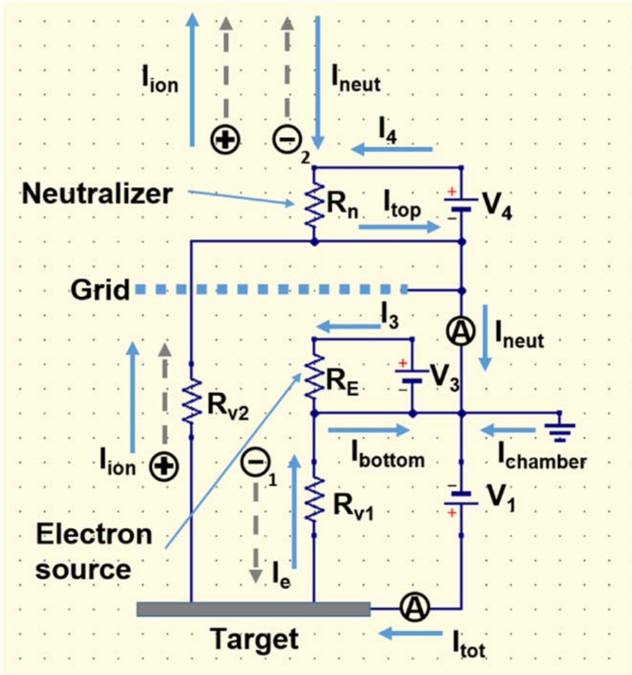

Figure 4. Circuit diagram of the experimental design. Resistors R_{E} and R_{n} represent the filaments of the electron source and the neutralizer, respectively. The resistor symbols R_{v1} and R_{v2}, on the other hand, are not from actual resistors but to represent the current path of the electron current I_{e} which heats the target from the electron source to the target and the current path of the ion current I_{ion}, respectively.

3. Experimental setup

Figure 4 displays equivalent circuit scheme of our MIT-MEB. Resistor R_{E} represents the filament of the electron source driven by V_3 with a current of I_3. Similarly, R_{n} represents the filament of the neutralizer driven by V_4 with a current of I_4. The resistor symbols R_{v1} and R_{v2}, on the other hand, are not from actual resistors but to represent the path of the electron current I_{e} from the electron source towards the target which heats the target, and the path of the ion current I_{ion}, respectively. The generated ions pass through the grid, and leave the thruster with unchanged ion current assuming that they do not collide with the grid. We needed to verify that the number of ions colliding with the grid was negligible. To this end, we measured I_{neut} with $V_4 = 0$, when no electrons were emitted from R_{n}. If accelerated ions had collided with the grid, the current I_{neut} would have been nonzero, but this was not the case. The role of the neutralizer is to sustain the process. Without it, the accelerated ions would leave the thruster and collide with the vacuum chamber. The current would flow back to the power supply through the grounding wire marked I_{chamber}. The neutralizer help balance I_{ion} by the electron current I_{neut}. As long as $I_{\mathrm{ion}} = I_{\mathrm{neut}}$, no net current leaves the thruster. In other words, the ion current from the target is equivalently connected to the neutralizer represented by R_{v2} and $I_{\mathrm{chamber}} = 0$. Therefore, $I_{\mathrm{top}} = I_4 + I_{\mathrm{neut}}$ and $I_{\mathrm{bottom}} = I_3 + I_{\mathrm{e}}$. Most importantly, when I_{ion} is fully balanced by I_{neut}, $I_{\mathrm{tot}} = I_{\mathrm{e}} + I_{\mathrm{ion}} = I_{\mathrm{e}} + I_{\mathrm{neut}}$. Both I_{tot} and I_{neut} were measured during the experiments, thus I_{e} that heats the target and I_{ion} could be also obtained. The evaporation rate of the zinc target was obtained by measuring the mass difference $\Delta M_{\mathrm{target}}$ and the time difference Δt before and after each experiment. If the ions leave the thruster normally, we can obtain the thrust F contributed from accelerated ions, the

Table 1. Measured voltages (V_1, V_3, V_4) and currents (I_{tot}, I_3, I_4, I_{neut}), mass differences ΔM_{target} under 5 min. The average evaporation rates $\dot{M}_{target}$ were calculated from dividing ΔM_{target} by 5 mins.

Conditions	I_{tot} (mA)	I_{neut} (mA)	V_3 (V)	I_3 (A)
5 kV/ 3 mA	3.0 ± 0.1	0.11 ± 0.02	1.83 ± 0.04	2.20 ± 0.10
1 kV/15 mA	15.5 ± 0.4	0.28 ± 0.02	2.02 ± 0.03	2.26 ± 0.03
Conditions	V_4 (V)	I_4 (A)	ΔM_{target} (g)	$\dot{M}_{target}$ (g/s)
5 kV/ 3 mA	2.30 ± 0.10	2.52 ± 0.01	$(70 \pm 10) \times 10^{-3}$	$(2.2 \pm 0.4) \times 10^{-4}$
1 kV/15 mA	2.42 ± 0.08	2.50 ± 0.01	$(5.0 \pm 1.0) \times 10^{-3}$	$(1.8 \pm 0.4) \times 10^{-5}$

ionized fraction β, and the power consumption Pw as follows:

$$F = I_{neut} \times \sqrt{\frac{2m_{ion}V_1}{q}}, \tag{3}$$

$$\beta = \frac{m_{ion}I_{neut}}{q}\left(\frac{\Delta M_{target}}{\Delta t}\right)^{-1}, \tag{4}$$

$$Pw = V_1 \times I_{tot} + V_3 \times I_3 + V_4 \times I_4 \tag{5}$$

where q is the charge of the ions. If metal vapor is fully ionized, the specific impulse can be determined by the ion exhaust speed, i.e. V_1 and m_{ion},

$$I_{sp,max} = \frac{1}{g}\sqrt{\frac{2V_1 q}{m_{ion}}}\ (\mathrm{s}). \tag{6}$$

For $V_1 = 5$ kV or 1 kV, the specific impulses for charged single zinc ions in our current desing are: $I_{sp} = 12400$ s and 5500 s, respectively. In our experiment, the ionization fraction was very little and the specific impulse we calculated from the ion exhaust speed was overestimated. We are not focusing on an implementation with high I_{sp} but only on proving our new concept.

We ran the experiments under two sets of conditions. Case 1: $V_1 = 5$ kV with $I_{tot} = 3$ mA. Case 2: $V_1 = 1$ kV with $I_{tot} = 15$ mA. We can see that the power consumptions were comparable. In Case 1, we first set $V_1 = 5$ kV and $V_3 = V_4 = 0$. At this moment, $I_{tot} = 0$ since the filament for the electron source was not heated, thus no electron current was generated. Increasing V_3 meant to heat the electron source. We reached $I_{tot} = 3$ mA. At this moment, $I_{neut} \equiv 0$ confirmed that the ions did not collide with the grid. The accelerated ions would leave the thruster and collide with the vacuum chamber, which was grounded. To eliminate that, we increased V_4 till I_{neut} reached the state of saturation, i.e. I_{ion} became balanced by I_{neut}. Afterwards, the system was kept running for five minutes, i.e. $\Delta t = 5$ min. We measured the mass difference ΔM_{target} of the target for calculating the evaporating rate. In Case 2, we followed the same process but setting $V_1 = 1$ kV with $I_{tot} = 15$ mA. As a result, we obtained the thrust, the ionization fraction, and the power consumption data for both cases.

4. Results

Table 1 lists the voltages (V_1, V_3, V_4), the currents (I_{tot}, I_3, I_4, I_{neut}), the mass differences ΔM_{target} and the corresponding average evaporation rates $\dot{M}_{target}$ in 5 min. The ionization fractions β and thrust F_{ion} were calculated by using equation (3) and (4), and listed in table 2. The total and the componentwise power consumption for both cases were also calculated and listed in table 3. The power consumptions were comparable in both cases. Energy used to heat filaments for emitting electrons in the ion source were 16% in Case 1 and 18% in Case 2. Since the ionization fractions were very low, the thrust contributed by exhausted vapor thermal velocity should not be ignored. Since zinc melted around the center region, we assume that the temperature of metal vapor was at least $T_{gas} \sim 420$ °C and use it to calculate the speed of the exhausted gas. Therefore, we estimate the thrust from the exhaust gas as

$$F_{gas} = \dot{M}_{target}(1 - \beta) \times \sqrt{\frac{2k_B T_{gas}}{m_{gas}}} \tag{7}$$

where $m_{gas} = m_{ion}$ is the atomic mass of the metal vapor. The average specific impulse is calculated as

$$I_{sp} \equiv \frac{F_{tot}}{\dot{M}_{target}\, g} \text{ where } F_{tot} = F_{ion} + F_{gas} \tag{8}$$

since not all metal vapor is ionized.

The experimental results showed that the evaporation rate $\dot{M}_{target}$ was one order higher in Case 1. The ion exhaust speed was also higher in Case 1. This means that Case 1 had higher heating efficiency. On the other hand, the ionization fraction was almost two orders lower in Case 1. The thrusts contributed by ions were comparable between the two cases. The total thrust, including the contribution from the exhaust gas, was an order higher in Case 1 due to a much higher mass flow rate. The average specific impulse I_{sp}, however, was lower in Case 1 due to the same reason. Although, thrust and average specific impulse do not compete well with existing ion thrusters yet, MIT-MEB has a great potential due to the advantages of using a metal propellant—high density, low cost, easy storage, and stability.

5. Discussion

We demonstrated the new concept of ion thrusters using metal propellant. Two different conditions with comparable power were tested. One using a higher voltage for accelerating thermal-emitted electrons in the ion source provided a higher

Table 2. The calculated ionization fraction β, the thrust F_{ion} contributed by accelerated ions, and the thrust F_{gas} contributed from zinc vapor. The specific impulse I_{sp} was calculated by equation (8).

Conditions	$\beta(\%)$	$F_{ion}(\mu N)$	$F_{gas}(\mu N)$	$I_{sp}(s)$
5 kV/ 3 mA	0.03 ± 0.01	9.0 ± 1.0	90 ± 40	47
1 kV/15 mA	1.1 ± 0.3	10.3 ± 0.7	7.0 ± 4.0	101

thrust. The thrust included the contribution of the accelerated ions and the outflow of the neutral metal vapor. The other one using a lower voltage provided a higher ionization fraction with a lower evaporation rate and thus a higher specific impulse I_{sp}.

There are several feasible directions to improve the utilities of our MIT-MEB. (i) better ion current measurements; (ii) reducing the power consumption via replacing the thermal-emitted electrons by field-emitted electrons for bombarding the target; (iii) lowering the electric potential V_1 in the ion source for increasing the ionization fraction; (iv) confining electrons in the ion source by using different magnets for increasing the ionization fraction.

(i) During the experiments, we expected that ion currents were only balanced in the neutralizer zone. However, ion currents may also be partially balanced in the ion source zone. In other words, the ion current I_{ion} is larger than I_{neut}, i.e. the measured ion current shown in table 1 is the lower bound. Instead of indirectly measuring the ion current by measuring I_{neut}, a Faraday cup can measure the ion current directly. Therefore, a Faraday cup will be used to measure the ion current.

(ii) In the present design, a lot of energy was used to heat filaments for emitting electrons in the ion source. One potential improvement is to replace the hot filament by a fine tungsten tip so that field-emitted electrons can be generated. Energy for heating filaments can be saved.

(iii) The ionization fraction needs to be increased. According to Tawara and Kato's measurements [17, 18] as shown in figure 5, the cross section of electron impact ionization peaks at ∼60 eV. Both the 1-keV and the 5-keV electrons on the target surface are too energetic for ionizing zinc vapor through electron impact ionization. Fortunately, electron energy can be reduced when electrons collide with the target. Each time electrons bombarding the target, ∼35% of the incident electrons are backscattered with half of the incident energy, i.e. ∼80% of the incident energy is deposited to the target [5–7]. Backscattered electrons leaving the target are pulled back to the target by the electric potential. They will bombard the target again and deposit more energy to it. Energies of electrons keep reducing every time when they collide and are backscattered by the target. Electron energy eventually reaches where the cross section of electron impact ionization peaks. However, the amount of electrons decreases dramatically during the process leading to a low ionization fraction. Besides the collision process, low energy electrons also present at the location near the hot filament where they are accelerated to only ∼60 eV. Therefore, zinc vapor can be ionized easier if it diffuses to the region close to the hot filament. However, only part of the zinc vapor diffuses to that region. Therefore, it is better to lower the incident electron energy to achieve a higher ionization fraction. It is why we saw a higher ionization fraction in Case 2. By reducing the electric potential V_1, electrons arriving the target surface may have the same energy to the energy of the peak cross section of electron impact ionization. Therefore, the ionization fraction can be increased. Further, to have the same power consumption with lower V_1, the electron current is higher. In other words, the electron density on the target surface will also increase. It is also beneficial to the ionization fraction. Therefore, optimizing the electric potential for achieving higher ionization fraction will be required.

(iv) Alternative way to increase the ionization fraction is to confine more electrons using different magnetic profile in the ion source region. The goal is that only few electrons are used to heat the target while most electrons are used for electron impact ionization. To prevent electrons from reaching the target surface, one can construct a mirror point of magnetic-mirror effect near the target surface. Therefore, only few electrons penetrating through the magnetic-mirror point will collide and heat the target. The zinc vapor is more likely to be ionized by electron impact ionization since most electrons remain in the ion source region. For example, the magnetic-field profile can be modified by adding a ring-type permanent magnet above the mesh that separates the ion source region and the accelerator region as shown in figure 6. The same magnetization to the existing magnet underneath the target was used in the simulation. An optimized magnetic-field profile can be obtained by changing the size, the geometry, the magnetization, and the position of the magnet.

(v) A single thruster can potentially work in two modes: high thrust mode vs high specific impulse mode. The thruster keeps $V_1 + V_2$ in figure 1 as a constant V_{tot} but with different ratio between V_1 and V_2. In the first mode, $V_1 \gg V_2$ is used to accelerate thermal-emitted electrons providing a higher evaporation rate and thus a higher thrust. It is closer to the electrothermal thruster category. In the second mode, V_1 is set to the voltage that can provide the highest ionization fraction. $V_2 = V_{tot} - V_1$ is used to accelerate ions providing a higher specific impulse. It is closer to the ion thruster category. By using a simple voltage divider that can adjust the ratio between V_1 and V_2, the thruster can be switched between two modes.

6. Conclusion

Metal ion thrusters using magnetron electron-beam bombardment (MIT-MEB) is a new concept of building ion thrusters using existing technology in the industry. We demonstrated the feasibility of building metal ion thrusters for

Table 3. The power consumption of the whole system and of each component. A significant portion of power was used for heating filaments for emitting electrons.

Conditions	Pw_{tot} (W)	Pw_{Ion} (W)	Pw_{filament} (W)	Pw_{Neut} (W)
5 kV/ 3 mA	24.8 ± 1.1	15.0 ± 0.5	4.0 ± 0.3	5.8 ± 0.3
1 kV/15 mA	26.2 ± 0.7	15.5 ± 0.4	4.6 ± 0.1	6.1 ± 0.2

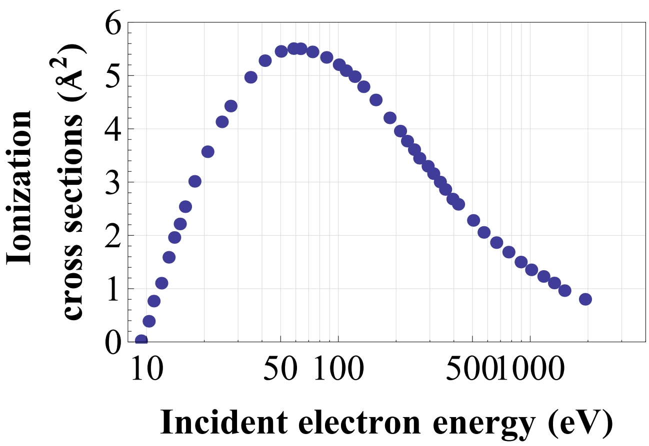

Figure 5. Cross section of electron impact ionization for zinc as measured by Tawara and Kato. It peaks at ∼60 eV. Courtesy of Ref. [18].

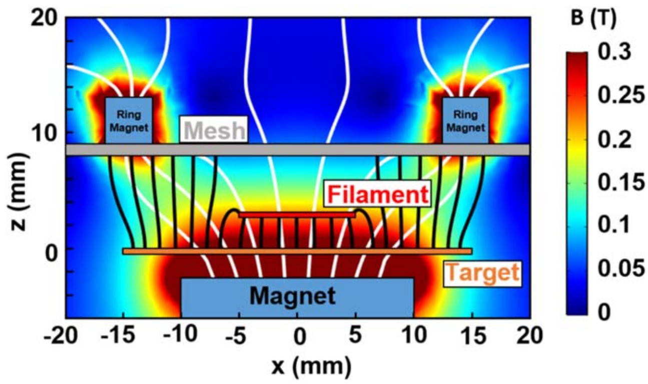

Figure 6. The simulated magnetic field with an additional ring-type magnet. White lines are magnetic field lines while black lines are electric field lines.

the first time. Metal propellants are in solid-state, high density, easy to store, and cheap. Therefore, they can be used in a small spacecraft for both attitude and orbit control and deep space exploration. These new ion thrusters open up the possibility of using small satellites for low earth orbit as well as deep space explorations using small satellites.

Acknowledgments

The authors would like to acknowledge Prof. Shu-Hui Chen and Prof. Hsu-Cheng Hsu in the Department of Chemistry and the Department of Photonics, National Cheng Kung University, Tainan, Taiwan, for lending them the precision scale and the 3-axis linear stage, respectively. The authors would also like to acknowledge Prof. Ming-Chieh Lin in the Department of Electrical and Biomedical Engineering, Hanyang University, Seoul, Korea, for his discussions on the physics of field-emitted electrons. The work was supported by the Ministry of Science and Technology (MOST), Taiwan, under Award Numbers 107-2628-E-006-006-MY2 and 105-2112-M-006-014-MY3.

ORCID iDs

Kuo-Yi Chen https://orcid.org/0000-0003-4855-2747
Po-Yu Chang https://orcid.org/0000-0002-2293-6980

References

[1] Goebel D M and Katz I 2008 *Fundamentals of Electric Propulsion: Ion and Hall Thrusters* 1st edn (New York: Wiley)
[2] Harsha K S S 2006 *Principles of Vapor Deposition of Thin Films* (Amsterdam: Elsevier Science)
[3] Darnell A J 1967 *The Characterization of High-Temperature Vapors* ed J L Margrave (Hoboken, NJ: John Wiley & Sons) Honig R E and Kramer D A 1969 *Vapor Pressure Data for the Solid and Liquid Elements* (Princeton, NJ: RCA Laboratories)
[4] Mattox D M 2010 *Handbook of Physical Vapor Deposition (PVD) Processing* 2nd edn (Norwich, NY: William Andrew)
[5] Kanaya K and Kawakatsu H 1972 Secondary electron emission due to primary and backscattered electrons *J. Phys. D: Appl. Phys.* **5** 1727–42
[6] Hunger H-J and Küchler L 1979 Measurements of the electron backscattering coefficient for quantitative EPMA in the energy range of 4 to 40 keV *Physica Status Solidi (a)* **56** K45–8
[7] Mukherjee J, Kumar V D, Yadav S P, Barnwal T A and Dikshit B 2016 Plasma diagnosis as a tool for the determination of the parameters of electron beam evaporation and sources of ionization *Meas. Sci. Technol.* **27** 075007
[8] Dushman S 1923 Electron emission from metals as a function of temperature *Phys. Rev.* **21** 623–36
[9] Richardson O W 1924 Electron emission from metals as a function of temperature *Phys. Rev.* **23** 153–5
[10] Crowell C R 1965 The Richardson constant for thermionic emission in Schottky barrier diodes *Solid-State Electron.* **8** 395–9
[11] Scholtz J J, Dijkkamp D and Schmitz R W A 1996 Secondary electron emission properties *Philips J. Res.* **50** 375–89 New Flat, Thin Display Technology

[12] Suszcynsky D M and Borovsky J E 1992 Modified Sternglass theory for the emission of secondary electrons by fast-electron impact *Phys. Rev.* A **45** 6424–8
[13] Yadav R K and Shanker R 2007 Contribution of backscattered electrons to the total electron yield produced in collisions of 8–28 keV electrons with tungsten *Pramana* **68** 507–15
[14] Kramida A, Ralchenko Y, Reader J and (NIST ASD Team) 2017 NIST Atomic Spectra Database (ver. 5.5.1) DOI: https://doi.org/10.18434/T4W30F
[15] Powell R W, Ho C Y and Liley P E 1966 *Thermal Conductivity of Selected Materials (National Standard Reference Data Series, NSRDS-NBS)* (Washington D.C: U.S. Dept. of Commerce, National Bureau of Standards)
[16] Linstrom P J and Mallard W G 2018 *Nist Chemistry Webbook, Nist Standard Reference Database Number 69* (Gaithersburg MD: National Institute of Standards and Technology) DOI: https://doi.org/10.18434/T4D303
[17] Tawara H and Kato T 1987 Total and partial ionization cross sections of atoms and ions by electron impact *At. Data Nucl. Data Tables* **36** 167–353
[18] Kaur J, Gupta D, Naghma R, Ghoshal D and Antony B 2015 Electron impact ionization cross sections of atoms *Can. J. Phys.* **93** 617–25